EUROPEAN ORGANIZATION FOR NUCLEAR RESEARCH

Measurement of α_s from Scaling Violations in Fragmentation Functions in e^+e^- Annihilation

The ALEPH Collaboration[1]

Abstract

A study of scaling violations in fragmentation functions performed by the ALEPH collaboration at LEP is presented. Data samples enriched in uds, c, b and gluon jets, respectively, together with measurements of the longitudinal and transverse inclusive cross sections are used to extract the fragmentation function for the gluon and for each flavour. The measurements are compared to data from experiments at energies between 22 GeV and 91 GeV and scaling violations consistent with QCD predictions are observed. From this, a measurement of the strong coupling constant $\alpha_s(M_Z) = 0.126 \pm 0.009$ is obtained.

[1]See next pages for the list of authors

The ALEPH Collaboration

D. Buskulic, D. Casper, I. De Bonis, D. Decamp, P. Ghez, C. Goy, J.-P. Lees, A. Lucotte, M.-N. Minard, P. Odier, B. Pietrzyk

Laboratoire de Physique des Particules (LAPP), IN^{2}P^3-CNRS, 74019 Annecy-le-Vieux Cedex, France

F. Ariztizabal, M. Chmeissani, J.M. Crespo, I. Efthymiopoulos, E. Fernandez, M. Fernandez-Bosman, V. Gaitan, Ll. Garrido,[15] M. Martinez, S. Orteu, A. Pacheco, C. Padilla, F. Palla, A. Pascual, J.A. Perlas, F. Sanchez, F. Teubert

Institut de Fisica d'Altes Energies, Universitat Autonoma de Barcelona, 08193 Bellaterra (Barcelona), Spain[7]

A. Colaleo, D. Creanza, M. de Palma, A. Farilla, G. Gelao, M. Girone, G. Iaselli, G. Maggi,[3] M. Maggi, N. Marinelli, S. Natali, S. Nuzzo, A. Ranieri, G. Raso, F. Romano, F. Ruggieri, G. Selvaggi, L. Silvestris, P. Tempesta, G. Zito

Dipartimento di Fisica, INFN Sezione di Bari, 70126 Bari, Italy

X. Huang, J. Lin, Q. Ouyang, T. Wang, Y. Xie, R. Xu, S. Xue, J. Zhang, L. Zhang, W. Zhao

Institute of High-Energy Physics, Academia Sinica, Beijing, The People's Republic of China[8]

G. Bonvicini, M. Cattaneo, P. Comas, P. Coyle, H. Drevermann, A. Engelhardt, R.W. Forty, M. Frank, R. Hagelberg, J. Harvey, R. Jacobsen,[24] P. Janot, B. Jost, J. Knobloch, I. Lehraus, C. Markou,[23] E.B. Martin, P. Mato, H. Meinhard, A. Minten, R. Miquel, T. Oest, P. Palazzi, J.R. Pater,[27] J.-F. Pusztaszeri, F. Ranjard, P. Rensing, L. Rolandi, D. Schlatter, M. Schmelling, O. Schneider, W. Tejessy, I.R. Tomalin, A. Venturi, H. Wachsmuth, W. Wiedenmann, T. Wildish, W. Witzeling, J. Wotschack

European Laboratory for Particle Physics (CERN), 1211 Geneva 23, Switzerland

Z. Ajaltouni, M. Bardadin-Otwinowska,[2] A. Barres, C. Boyer, A. Falvard, P. Gay, C. Guicheney, P. Henrard, J. Jousset, B. Michel, S. Monteil, J-C. Montret, D. Pallin, P. Perret, F. Podlyski, J. Proriol, J.-M. Rossignol, F. Saadi

Laboratoire de Physique Corpusculaire, Université Blaise Pascal, IN^{2}P^3-CNRS, Clermont-Ferrand, 63177 Aubière, France

T. Fearnley, J.B. Hansen, J.D. Hansen, J.R. Hansen, P.H. Hansen, B.S. Nilsson

Niels Bohr Institute, 2100 Copenhagen, Denmark[9]

A. Kyriakis, E. Simopoulou, I. Siotis, A. Vayaki, K. Zachariadou

Nuclear Research Center Demokritos (NRCD), Athens, Greece

A. Blondel,[21] G. Bonneaud, J.C. Brient, P. Bourdon, L. Passalacqua, A. Rougé, M. Rumpf, R. Tanaka, A. Valassi,[31] M. Verderi, H. Videau

Laboratoire de Physique Nucléaire et des Hautes Energies, Ecole Polytechnique, IN^{2}P^3-CNRS, 91128 Palaiseau Cedex, France

D.J. Candlin, M.I. Parsons

Department of Physics, University of Edinburgh, Edinburgh EH9 3JZ, United Kingdom[10]

E. Focardi, G. Parrini

Dipartimento di Fisica, Università di Firenze, INFN Sezione di Firenze, 50125 Firenze, Italy

M. Corden, M. Delfino,[12] C. Georgiopoulos, D.E. Jaffe

Supercomputer Computations Research Institute, Florida State University, Tallahassee, FL 32306-4052, USA [13,14]

A. Antonelli, G. Bencivenni, G. Bologna,[4] F. Bossi, P. Campana, G. Capon, V. Chiarella, G. Felici, P. Laurelli, G. Mannocchi,[5] F. Murtas, G.P. Murtas, M. Pepe-Altarelli

Laboratori Nazionali dell'INFN (LNF-INFN), 00044 Frascati, Italy

S.J. Dorris, A.W. Halley, I. ten Have,[6] I.G. Knowles, J.G. Lynch, W.T. Morton, V. O'Shea, C. Raine, P. Reeves, J.M. Scarr, K. Smith, M.G. Smith, A.S. Thompson, F. Thomson, S. Thorn, R.M. Turnbull

Department of Physics and Astronomy, University of Glasgow, Glasgow G12 8QQ,United Kingdom[10]

U. Becker, O. Braun, C. Geweniger, G. Graefe, P. Hanke, V. Hepp, E.E. Kluge, A. Putzer, B. Rensch, M. Schmidt, J. Sommer, H. Stenzel, K. Tittel, S. Werner, M. Wunsch

Institut für Hochenergiephysik, Universität Heidelberg, 69120 Heidelberg, Fed. Rep. of Germany[16]

R. Beuselinck, D.M. Binnie, W. Cameron, D.J. Colling, P.J. Dornan, N. Konstantinidis, L. Moneta, A. Moutoussi, J. Nash, G. San Martin, J.K. Sedgbeer, A.M. Stacey

Department of Physics, Imperial College, London SW7 2BZ, United Kingdom[10]

G. Dissertori, P. Girtler, E. Kneringer, D. Kuhn, G. Rudolph

Institut für Experimentalphysik, Universität Innsbruck, 6020 Innsbruck, Austria[18]

C.K. Bowdery, T.J. Brodbeck, P. Colrain, G. Crawford, A.J. Finch, F. Foster, G. Hughes, T. Sloan, E.P. Whelan, M.I. Williams

Department of Physics, University of Lancaster, Lancaster LA1 4YB, United Kingdom[10]

A. Galla, A.M. Greene, K. Kleinknecht, G. Quast, J. Raab, B. Renk, H.-G. Sander, R. Wanke, C. Zeitnitz

Institut für Physik, Universität Mainz, 55099 Mainz, Fed. Rep. of Germany[16]

J.J. Aubert, A.M. Bencheikh, C. Benchouk, A. Bonissent,[21] G. Bujosa, D. Calvet, J. Carr, C. Diaconu, F. Etienne, M. Thulasidas, D. Nicod, P. Payre, D. Rousseau, M. Talby

Centre de Physique des Particules, Faculté des Sciences de Luminy, IN^{2}P^3-CNRS, 13288 Marseille, France

I. Abt, R. Assmann, C. Bauer, W. Blum, D. Brown,[24] H. Dietl, F. Dydak,[21] G. Ganis, C. Gotzhein, K. Jakobs, H. Kroha, G. Lütjens, G. Lutz, W. Männer, H.-G. Moser, R. Richter, A. Rosado-Schlosser, S. Schael, R. Settles, H. Seywerd, U. Stierlin,[2] R. St. Denis, G. Wolf

Max-Planck-Institut für Physik, Werner-Heisenberg-Institut, 80805 München, Fed. Rep. of Germany[16]

R. Alemany, J. Boucrot, O. Callot, A. Cordier, F. Courault, M. Davier, L. Duflot, J.-F. Grivaz, Ph. Heusse, M. Jacquet, D.W. Kim,[19] F. Le Diberder, J. Lefrançois, A.-M. Lutz, G. Musolino, I. Nikolic, H.J. Park, I.C. Park, M.-H. Schune, S. Simion, J.-J. Veillet, I. Videau

Laboratoire de l'Accélérateur Linéaire, Université de Paris-Sud, IN^{2}P^3-CNRS, 91405 Orsay Cedex, France

D. Abbaneo, P. Azzurri, G. Bagliesi, G. Batignani, S. Bettarini, C. Bozzi, G. Calderini, M. Carpinelli, M.A. Ciocci, V. Ciulli, R. Dell'Orso, R. Fantechi, I. Ferrante, L. Foà,[1] F. Forti, A. Giassi, M.A. Giorgi, A. Gregorio, F. Ligabue, A. Lusiani, P.S. Marrocchesi, A. Messineo, G. Rizzo, G. Sanguinetti, A. Sciabà, P. Spagnolo, J. Steinberger, R. Tenchini, G. Tonelli,[26] G. Triggiani, C. Vannini, P.G. Verdini, J. Walsh

Dipartimento di Fisica dell'Università, INFN Sezione di Pisa, e Scuola Normale Superiore, 56010 Pisa, Italy

A.P. Betteridge, G.A. Blair, L.M. Bryant, F. Cerutti, Y. Gao, M.G. Green, D.L. Johnson, T. Medcalf, Ll.M. Mir, P. Perrodo, J.A. Strong

Department of Physics, Royal Holloway & Bedford New College, University of London, Surrey TW20 OEX, United Kingdom[10]

V. Bertin, D.R. Botterill, R.W. Clifft, T.R. Edgecock, S. Haywood, M. Edwards, P. Maley, P.R. Norton, J.C. Thompson

Particle Physics Dept., Rutherford Appleton Laboratory, Chilton, Didcot, Oxon OX11 OQX, United Kingdom[10]

B. Bloch-Devaux, P. Colas, H. Duarte, S. Emery, W. Kozanecki, E. Lançon, M.C. Lemaire, E. Locci, B. Marx, P. Perez, J. Rander, J.-F. Renardy, A. Rosowsky, A. Roussarie, J.-P. Schuller, J. Schwindling, D. Si Mohand, A. Trabelsi, B. Vallage

CEA, DAPNIA/Service de Physique des Particules, CE-Saclay, 91191 Gif-sur-Yvette Cedex, France[17]

R.P. Johnson, H.Y. Kim, A.M. Litke, M.A. McNeil, G. Taylor

Institute for Particle Physics, University of California at Santa Cruz, Santa Cruz, CA 95064, USA[22]

A. Beddall, C.N. Booth, R. Boswell, S. Cartwright, F. Combley, I. Dawson, A. Koksal, M. Letho, W.M. Newton, C. Rankin, L.F. Thompson

Department of Physics, University of Sheffield, Sheffield S3 7RH, United Kingdom[10]

A. Böhrer, S. Brandt, G. Cowan, E. Feigl, C. Grupen, G. Lutters, J. Minguet-Rodriguez, F. Rivera,[25] P. Saraiva, L. Smolik, F. Stephan

Fachbereich Physik, Universität Siegen, 57068 Siegen, Fed. Rep. of Germany[16]

M. Apollonio, L. Bosisio, R. Della Marina, G. Giannini, B. Gobbo, F. Ragusa[20]

Dipartimento di Fisica, Università di Trieste e INFN Sezione di Trieste, 34127 Trieste, Italy

J. Rothberg, S. Wasserbaech

Experimental Elementary Particle Physics, University of Washington, WA 98195 Seattle, U.S.A.

S.R. Armstrong, L. Bellantoni,[30] P. Elmer, Z. Feng, D.P.S. Ferguson, Y.S. Gao, S. González, J. Grahl, J.L. Harton,[28] O.J. Hayes, H. Hu, P.A. McNamara III, J.M. Nachtman, W. Orejudos, Y.B. Pan, Y. Saadi, M. Schmitt, I.J. Scott, V. Sharma,[29] J.D. Turk, A.M. Walsh, Sau Lan Wu, X. Wu, J.M. Yamartino, M. Zheng, G. Zobernig

Department of Physics, University of Wisconsin, Madison, WI 53706, USA[11]

---

[1] Now at CERN, 1211 Geneva 23, Switzerland.
[2] Deceased.
[3] Now at Dipartimento di Fisica, Università di Lecce, 73100 Lecce, Italy.
[4] Also Istituto di Fisica Generale, Università di Torino, Torino, Italy.
[5] Also Istituto di Cosmo-Geofisica del C.N.R., Torino, Italy.
[6] Now at TSM Business School, Enschede, The Netherlands.
[7] Supported by CICYT, Spain.
[8] Supported by the National Science Foundation of China.
[9] Supported by the Danish Natural Science Research Council.
[10] Supported by the UK Particle Physics and Astronomy Research Council.
[11] Supported by the US Department of Energy, contract DE-AC02-76ER00881.
[12] On leave from Universitat Autonoma de Barcelona, Barcelona, Spain.
[13] Supported by the US Department of Energy, contract DE-FG05-92ER40742.
[14] Supported by the US Department of Energy, contract DE-FC05-85ER250000.
[15] Permanent address: Universitat de Barcelona, 08208 Barcelona, Spain.
[16] Supported by the Bundesministerium für Forschung und Technologie, Fed. Rep. of Germany.
[17] Supported by the Direction des Sciences de la Matière, C.E.A.
[18] Supported by Fonds zur Förderung der wissenschaftlichen Forschung, Austria.
[19] Permanent address: Kangnung National University, Kangnung, Korea.
[20] Now at Dipartimento di Fisica, Università di Milano, Milano, Italy.
[21] Also at CERN, 1211 Geneva 23, Switzerland.
[22] Supported by the US Department of Energy, grant DE-FG03-92ER40689.
[23] Now at University of Athens, 157-71 Athens, Greece.
[24] Now at Lawrence Berkeley Laboratory, Berkeley, CA 94720, USA.
[25] Partially supported by Colciencias, Colombia.
[26] Also at Istituto di Matematica e Fisica, Università di Sassari, Sassari, Italy.
[27] Now at Schuster Laboratory, University of Manchester, Manchester M13 9PL, UK.
[28] Now at Colorado State University, Fort Collins, CO 80523, USA.
[29] Now at University of California at San Diego, La Jolla, CA 92093, USA.
[30] Now at Fermi National Accelerator Laboratory, Batavia, IL 60510, USA.
[31] Supported by the Commission of the European Communities, contract ERBCHBICT941234.

1 Introduction

The study of scaling violations in structure functions in deep-inelastic lepton-nucleon scattering played a fundamental role in establishing Quantum Chromodynamics (QCD) as the theory of strong interactions. QCD predicts similar scaling violations in the fragmentation functions of quarks and gluons. In an electron-positron collider this translates into the fact that the distributions of the scaled-energy $x \equiv 2E/\sqrt{s}$ of final state particles in hadronic events depend on the centre-of-mass energy $\sqrt{s}$. These scaling violations come about because with increasing $\sqrt{s}$ more phase space for gluon radiation and thus final state particle production becomes available, leading to a softer x-distribution. As the probability for gluon radiation is proportional to the strong coupling constant, a measurement of the scaled-energy distributions at different centre-of-mass energies compared to the QCD prediction allows to determine the only free parameter of QCD, α_s.

In principle, variations with energy of the x distributions would establish the existence of scaling violations and allow the determination of α_s. However, the fact that the final state flavour composition depends strongly on the centre-of-mass energy (abundance of u-type quarks at PEP and PETRA energies and majority of d-type quarks at LEP energies), and that the fragmentation functions depend on the quark mass, means that the effect would be biased by differences between fragmentation functions for the different quark flavours. Therefore, in order to disentangle scaling violations arising from gluon radiation from effects due to the changing flavour composition independently of Monte Carlo modeling, final state flavour identification is needed.

The work presented here uses inclusive scaled-energy distributions of stable charged particles measured at PEP, PETRA, TRISTAN and LEP together with ALEPH measurements of the distributions in bottom-, charm- and light-quark enriched samples, an inclusive sample, and a gluon jet sample. These data, obtained in 1992 and 1993, correspond to approximately 40 pb^{-1} taken at a centre-of-mass energy around 91.2 GeV. They amount to close to 1.2 million hadronic decays of the Z.

Section 2 describes the theoretical framework of this analysis, which is based on the Dokshitzer-Gribov-Lipatov-Altarelli-Parisi (DGLAP) evolution equations [1] with splitting kernels and coefficient functions computed to next-to-leading order [2, 3]. The event selection, flavour tagging and data analysis are presented in section 3. Results are discussed in section 4 and conclusions are given in section 5. An earlier investigation of scaling violations in e^+e^- collisions has been carried out by the DELPHI Collaboration [4], in which the analysis was based on $\mathcal{O}(\alpha_s^2)$ matrix elements as implemented in the JETSET model [5].

2 Theoretical Prediction

The general form for the inclusive distribution of x and polar angle θ with respect to the beam axis is given by [6]:

$$\frac{d^2\sigma(s)}{dx\, d\cos\theta} = \frac{3}{8}(1+\cos^2\theta)\,\frac{d\sigma^T(s)}{dx} + \frac{3}{4}\sin^2\theta\,\frac{d\sigma^L(s)}{dx} + \frac{3}{4}\cos\theta\,\frac{d\sigma^A(s)}{dx},$$

where T, L and A refer to the transverse, longitudinal and asymmetric cross sections. Integrating over $\cos\theta$ one obtains the inclusive cross section

$$\frac{d\sigma(s)}{dx} = \frac{d\sigma^T(s)}{dx} + \frac{d\sigma^L(s)}{dx}$$

which carries most of the weight in this analysis. The total cross section is dominated by the transverse component. The longitudinal one arises from QCD corrections and, as described below, is only used to constrain the gluon fragmentation function. The cross sections are related to fragmentation functions D_i, $i = u, d, s, c, b$, for quarks and D_g for gluons, which describe the momentum spectrum of final state particles from a single parton, by a convolution with coefficient functions C_q, C_g:

$$\begin{aligned}\frac{d\sigma(s)}{dx} &= 2\sigma_0(s)\int_x^1 \frac{dz}{z} C_q(z, \alpha_s(\mu_F), \mu_F^2/s) \sum_{i=u,d,s,c,b} w_i(s)\, D_i(x/z, \mu_F^2) \\ &+ 2\sigma_0(s)\int_x^1 \frac{dz}{z} C_g(z, \alpha_s(\mu_F), \mu_F^2/s)\, D_g(x/z, \mu_F^2)\ . \end{aligned} \tag{1}$$

Here $\sigma_0(s)$ is the Born cross section at the centre-of-mass energy $\sqrt{s}$ and w_i is the relative electroweak cross section for the production of primary quarks of type i. The scale μ_F is an arbitrary factorization scale where the fragmentation functions are evaluated. The fragmentation functions themselves cannot be calculated within perturbative QCD, but once they are fixed at some parametrization scale $\sqrt{s_0}$, their energy evolution is predicted. The coefficient functions are known to next-to-leading order, $\mathcal{O}(\alpha_s)$. At leading order only $C_q = \delta(1-z)$ is different from zero, i.e. the cross section is proportional to the weighted sum of the quark fragmentation functions.

The QCD scaling violations are described by the DGLAP evolution equations

$$\frac{dD_j(x,s)}{d\ln s} = \sum_{i=u,d,s,c,b,g} \int_x^1 \frac{dz}{z} P_{ij}(z, \alpha_s(\mu_R), \mu_R^2/s)\, D_i(x/z, s)\ , \tag{2}$$

where μ_R is the renormalization scale. The splitting kernels P_{ij} are known to next-to-leading order $\mathcal{O}(\alpha_s^2)$. The energy evolution of the strong coupling constant is described by the same two-loop formula that was used in ref. [7]. Both the coefficient functions and the splitting kernels in the $\overline{\rm MS}$ scheme can be found, for example, in ref. [6]. For the analysis presented in this paper the scales μ_R and μ_F are varied around the natural scale $\sqrt{s}$ as in ref. [7], because the integration of the next-to-leading order evolution equations implies an all-orders resummation of leading and next-to-leading logarithms. Consequently, very small scales which to some extent do mimic this resummation are not needed. The evolution equation is solved numerically using the standard Runge-Kutta method.

Because the fragmentation functions depend on the quark mass, and the relative cross section for each flavour depends on $\sqrt{s}$, a measurement of α_s from scaling violations in inclusive momentum distributions requires the knowledge of the fragmentation functions for all quark flavours at one energy. Equations (1) and (2) show that the gluon fragmentation function is also needed. Information about the various quark flavours can be extracted from the data, if the flavour composition of the data sample is controlled experimentally by using appropriate tagging techniques. A direct measurement of the gluon fragmentation function can be obtained from three-jet events, where jets from well separated gluons are tagged by default when the other two jets contain long-lived particles. Additional information can be extracted from the longitudinal and transverse cross sections which are related to the gluon fragmentation function according to [6]

$$\frac{1}{\sigma_{tot}}\frac{d\sigma^L}{dx} = \frac{\alpha_s}{2\pi}\int_x^1 \frac{dz}{z}\left[\frac{1}{\sigma_{tot}}\frac{d\sigma^T}{dz} + 4\left(\frac{z}{x}-1\right) D_g(z)\right] + \mathcal{O}(\alpha_s^2), \tag{3}$$

with as yet uncalculated terms $\mathcal{O}(\alpha_s^2)$. Truncating the above expression at $\mathcal{O}(\alpha_s)$, the parameter α_s becomes an effective leading-order coupling constant which must not be confused with the next-to-leading order running coupling constant appearing in eqs. (1),(2). Because of this, it will be referred to as β_s in the following.

The formalism developed above describes only the perturbative component of the scaling violations. Corrections due to resonance decays that scale like m^2/s, quark-mass effects and non-perturbative effects are discussed in detail in ref. [6]. The latter manifest themselves as power-law corrections of $\mathcal{O}(1/\sqrt{s^k})$ to the logarithmic scaling violations expected from perturbative QCD. While the coefficient k is known to be $k = 2$ for deep-inelastic scattering experiments, there is no clear theoretical prediction for the case of scaling violations in fragmentation functions. Phenomenological arguments [6], however, suggest that it may be $k = 1$. A simple way of incorporating non-perturbative effects is by changing variables and relating the perturbative variable x to the measured quantity x' through a function $x = g(x')$. The ansatz

$$x = x' + h_0 \left(\frac{1}{\sqrt{s}} - \frac{1}{\sqrt{s_0}} \right), \tag{4}$$

with one effective parameter h_0, supported by Monte Carlo studies, is used to parametrize all power-law corrections over the energy range between 22 GeV and 91.2 GeV covered by the data analysed here.

The functional form eq.(4) implies that at the parametrization scale $\sqrt{s_0}$ all non-perturbative effects are absorbed into the fragmentation functions.

3 Data Analysis

The ALEPH detector, which provides both tracking and calorimetric information over almost the full solid angle, is described in detail elsewhere [8]. The momentum of charged particles is given by a fit to the information provided by the three tracking devices: a double-sided silicon microvertex detector (VDET), an eight-layer axial-wire chamber (ITC) and a large time projection chamber (TPC). The momentum resolution achieved in the combined fit is $\Delta p/p = 0.0006\, p/(\mathrm{GeV}/c) \oplus 0.005$, where the two contributions are to be added in quadrature. A detailed description of the performance of the detector can be found in ref. [9].

The event and charged track selections follow the method presented in ref. [10]. All charged particles are assigned the pion mass. The transverse momentum of each charged track has to be greater than 200 MeV/c. The selection efficiency for hadronic Z decays is 77%. The only sizable inefficiency is introduced by requiring the sphericity axis of each event to be more than 35 degrees away from the beam line, thus ensuring that the event is well contained in the detector. The main background comes from $\tau^+\tau^-$ events and amounts to about 0.3%. Although the background is small, it is concentrated at high values of x. It therefore could affect the measurement and it is subtracted bin by bin in the scaled energy distribution using a Monte Carlo simulation [11]. The distribution then is corrected using a hadronic event generator based on DYMU3 [12] and JETSET 7.3 [5] with parameters adjusted to describe the ALEPH data [10], for the effects of geometrical acceptance, detector efficiency and resolution, decays of long-lived particles (with

$\tau > 1$ ns), secondary interactions and initial state photon radiation. The raw distributions are corrected bin by bin according to the method explained in ref. [10].

The exclusive distributions are measured from samples enriched in bottom, charm and light quarks (u, d, s). These samples are prepared using a lifetime tag based on the measurement of the impact parameter of the charged tracks and on the probability of each trajectory to originate at the interaction point. The algorithm is described in detail in ref. [13]. From individual probabilities an overall probability P_h is computed that a given collection of tracks has no products from long-lived particles. Requiring P_h to be less than a given value increases the likelihood that the event contains long-lived particles.

In order to reduce the bias introduced by the tagging algorithm (which is more efficient for events with large charged multiplicity) the event is divided into two hemispheres according to the thrust axis and the algorithm is applied only to the tracks of the first hemisphere. If that hemisphere passes the selection cut, the other one is used to measure the charged particle spectrum, weighting each track with a factor of two. The cross sections are normalized to the number of accepted hemispheres. Finally, since the two hemispheres are almost independent, the procedure is repeated with the tag applied to the second hemisphere. Residual correlations between the hemispheres are taken into account in the correction procedure.

A sample enriched with bottom-quark events is obtained requiring $P_h < 0.001$, which results in a b-identification efficiency of about 32.5%. The flavour composition of the tagged sample is 90.5% of bottom quarks, 7.3% of charm quarks and 2.2% of light quarks, according to the Monte Carlo. It has been checked [13] that the Monte Carlo efficiencies and purities agree well with those in the data.

Using the same technique, a light-quark enriched sample has been prepared. In this case, the hemisphere probability to come from the interaction point is required to be $P_h > 0.1$. The light-quark efficiency is about 74%, and the tagged sample consists of 78.9% light-quark events, 14.5% charm events and 6.6% bottom events.

A sample enriched in c-quark events is obtained requiring $0.001 < P_h < 0.07$. In order to increase the purity the global hemisphere-shape variables described in ref. [14] are used. There, a likelihood is formed for a hemisphere to belong to a bottom event, based on two shape variables, moment of inertia and lateral mass [14]. The first one is closely related to a hemisphere boost sphericity, while the second one sums the boosted momenta of particles in one hemisphere that are close to its axis. The value of this likelihood must be below 0.2. The final sample consists of 35.1% charm events, 26.7% bottom events and 38.2% light-quark events. The efficiency for c-quark tagging is about 9%.

At next-to-leading order accuracy the gluon fragmentation function also appears in the evolution equations. Two methods have been used to measure it. In the first case, the above-mentioned b-tagging algorithm is applied to individual jets in events with three well separated jets in order to tag the two b-quark jets and, therefore, the gluon jet. Then, the inclusive charged-particle momentum distribution of the gluon jet, scaled to its energy, is measured. The procedure is described in detail in ref. [15] and the results are taken from there. This method is most suitable for rather large values of the scaled energy, above $x = 0.3$, because of the cleaner association of particles to jets.

The second method to obtain information on the gluon fragmentation function is based on

eq. (3). The longitudinal and transverse cross sections are measured by weighting the double-differential cross section with respect to x and $\cos\theta$ with the appropriate weight to project onto the $(1+\cos^2\theta)$ component (transverse) or the $\sin^2\theta$ component (longitudinal):

$$\frac{d\sigma^{L,T}}{dx} = \int_{-v}^{+v} d\cos\theta \, W_{L,T}(\cos\theta, v) \, \frac{d^2\sigma}{dx \, d\cos\theta}$$

with [6]

$$W_L(\cos\theta, v) = \left[v^2\left(5+3v^2\right) - 5\cos^2\theta\left(3+v^2\right)\right]/4v^5$$

and

$$W_T(\cos\theta, v) = \left[5\cos^2\theta\left(3-v^2\right) - v^2\left(5-3v^2\right)\right]/2v^5$$

the longitudinal and transverse projectors, respectively, and v defining the detector acceptance, which is considered to be constant in the range $|\cos\theta| < v = 0.94$. For the measurement of the longitudinal and transverse distributions the requirement on the sphericity axis is removed, as it would introduce a strong $\cos\theta$ dependence in the track selection efficiency. Even without this requirement, the track reconstruction efficiency degrades at low polar angles, especially for high-momentum tracks. This effect is taken into account in the correction procedure, which is identical to that used for the other distributions. This leads to larger corrections, but these are well understood, with the uncertainty in the reconstruction efficiency taken into account into the systematic errors.

Systematic uncertainties in all the distributions coming from possible discrepancies between the real detector performance and the simulated one are estimated by varying the cuts applied in the track and event selection. The maximum variation of a given bin is taken to be an uncorrelated experimental systematic uncertainty [10]. The analysis of these variations shows no significant correlation among different bins in the x distribution. The track reconstruction efficiency is well simulated in the Monte Carlo, with the inefficiencies at low polar angles known within 10% of their value. To probe the sensitivity of the longitudinal cross section to the track reconstruction efficiency, the $\cos\theta$ range was varied from $v = 0.94$ to $v = 0.90$ and the resulting difference taken as an additional systematic error. On top of this, a 1% normalization error is assigned to each distribution, in accordance with the findings of ref. [16]. Systematic uncertainties specific to the flavour tagging procedures are treated separately and are described in section 4.

The dependence on the hadron production model used to correct the data for detector effects is estimated by computing simplified correction factors [10] (with only acceptance cuts) using three different models: the one used for the corrections [5], NLLJET [17] and ARIADNE 2.3 [18]. The full spread between the values obtained correcting with the three models is added in quadrature to the bin-by-bin systematic error. For the longitudinal cross section this model dependence constitutes the dominant systematic uncertainty. The model corresponding to the HERWIG 5.6 program [19] has not been used because it has been found to describe very poorly the features of the scaled energy distribution at large values of x (above 0.3).

Figure 1 plots the measured ALEPH distributions. One clearly sees the difference between light and heavy flavour enriched samples. The errors include all bin-to-bin errors (statistical and systematic) added in quadrature as well as an overall 1% normalization error. Systematic errors dominate everywhere. The agreement with the JETSET 7.3 [5] Monte Carlo prediction

is reasonable for all distributions and x regions. The transverse distribution is almost identical to the unweighted one for all flavours and is not shown. The numerical values for the inclusive, transverse and longitudinal cross sections are given in Table 1. The longitudinal and transverse distributions agree with the recent measurement by the OPAL Collaboration [20].

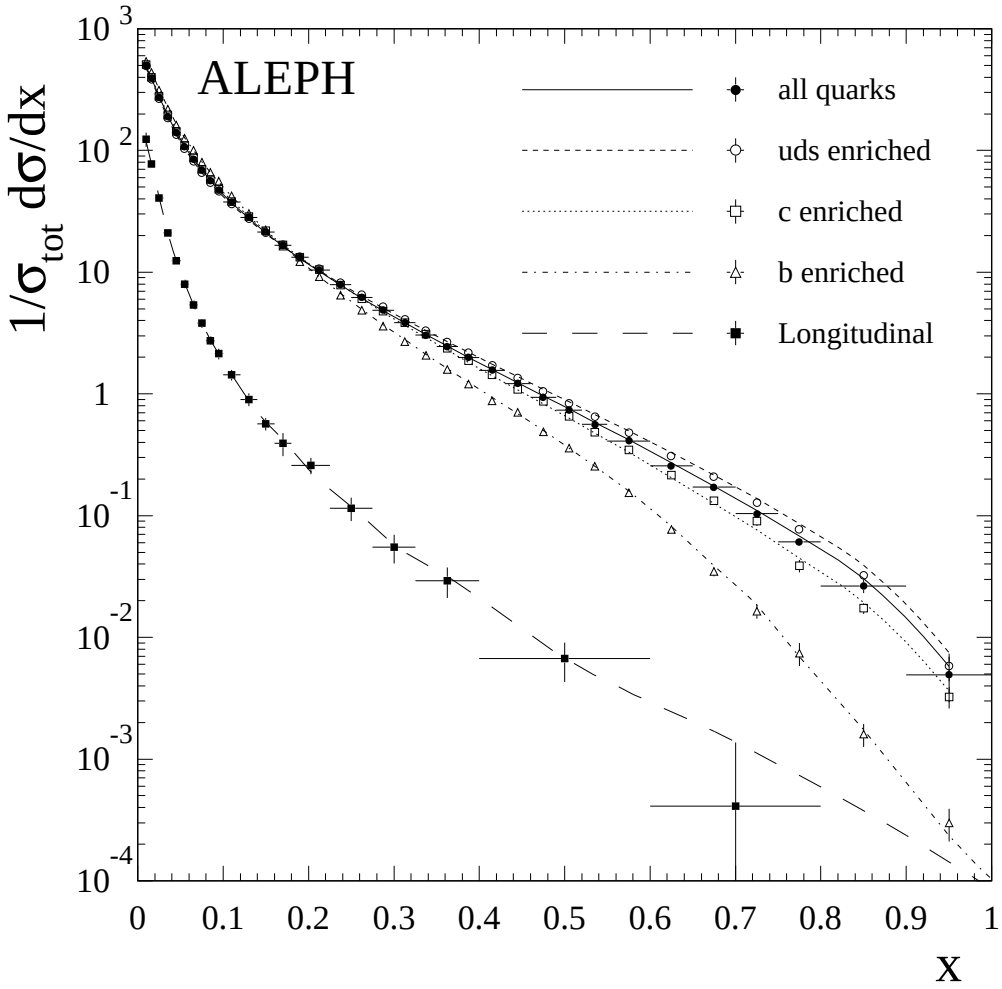

Figure 1: Measured scaled-energy distributions corrected for detector effects (symbols) and comparison with the predictions from JETSET 7.3 (curves). The distributions are normalized to the total number of events. Error bars include statistical and systematic uncertainties. The same binning is used for the inclusive and flavour-tagged distributions.

In addition to the ALEPH data, inclusive charged particle spectra from TASSO [21] at $\sqrt{s}$ = 22, 35 and 45 GeV, MARK II [22] and TPC/2γ [23] at $\sqrt{s}$ = 29 GeV, CELLO [24] at $\sqrt{s}$ = 35 GeV, AMY [25] at $\sqrt{s}$ = 55 GeV and DELPHI [4] at $\sqrt{s}$ = 91.2 GeV have been used in the analysis. Lower-energy data have been discarded because of the possible larger size of the power-law corrections. In all those measurements, x was defined as $x = 2p/\sqrt{s}$. The difference with the ALEPH definition, $x = 2E/\sqrt{s}$, leads to negligible power-law corrections in the range $0.1 < x < 0.8$, used for the fit in the following section.

Interval	Total	Transverse	Longitudinal
0.008–0.012	501.3 ±0.4 ±7.8	377.2 ±0.9 ±52.5	123.6 ±0.5 ±16.4
0.012–0.020	392.69 ±0.24 ±0.97	314.9 ±0.5 ± 4.4	77.2 ±0.3 ± 2.8
0.028–0.030	274.81 ±0.18 ±0.99	234.5 ±0.4 ± 2.4	40.6 ±0.2 ± 1.6
0.030–0.040	191.05 ±0.15 ±0.48	170.1 ±0.3 ± 1.0	21.1 ±0.1 ± 1.2
0.040–0.050	139.94 ±0.13 ±0.44	127.50 ±0.25 ± 0.72	12.42 ±0.12 ± 0.81
0.050–0.060	107.33 ±0.11 ±0.30	99.29 ±0.22 ± 0.61	8.00 ±0.10 ± 0.58
0.060–0.070	85.09 ±0.10 ±0.17	79.61 ±0.19 ± 0.60	5.40 ±0.09 ± 0.40
0.070–0.080	68.96 ±0.09 ±0.19	65.23 ±0.17 ± 0.42	3.81 ±0.08 ± 0.31
0.080–0.090	56.80 ±0.08 ±0.13	54.09 ±0.16 ± 0.39	2.74 ±0.07 ± 0.20
0.090–0.100	47.875 ±0.075 ±0.095	45.72 ±0.14 ± 0.23	2.14 ±0.06 ± 0.20
0.100–0.120	37.655 ±0.047 ±0.074	36.22 ±0.09 ± 0.16	1.43 ±0.04 ± 0.14
0.120–0.140	28.061 ±0.041 ±0.046	27.12 ±0.08 ± 0.31	0.90 ±0.03 ± 0.10
0.140–0.160	21.389 ±0.035 ±0.054	20.77 ±0.07 ± 0.11	0.569 ±0.026 ± 0.060
0.160–0.180	16.661 ±0.031 ±0.042	16.32 ±0.06 ± 0.16	0.393 ±0.024 ± 0.082
0.180–0.200	13.233 ±0.028 ±0.027	11.323 ±0.033 ± 0.089	0.259 ±0.012 ± 0.037
0.200–0.225	10.376 ±0.022 ±0.023		
0.225–0.250	7.928 ±0.019 ±0.020	6.943 ±0.025 ± 0.055	0.115 ±0.008 ± 0.024
0.250–0.275	6.197 ±0.017 ±0.016		
0.275–0.300	4.874 ±0.015 ±0.012	4.319 ±0.020 ± 0.027	0.055 ±0.005 ± 0.013
0.300–0.325	3.862 ±0.014 ±0.013		
0.325–0.350	3.055 ±0.012 ±0.018	2.474 ±0.012 ± 0.018	0.0293 ±0.0032 ± 0.0076
0.350–0.375	2.461 ±0.011 ±0.009		
0.375–0.400	1.995 ±0.010 ±0.011		
0.400–0.430	1.5555±0.0079±0.0059	0.8439±0.0043± 0.0068	0.0067 ±0.0007 ± 0.0023
0.430–0.460	1.2122±0.0070±0.0081		
0.460–0.490	0.9401±0.0061±0.0051		
0.490–0.520	0.7346±0.0054±0.0091		
0.520–0.550	0.5634±0.0047±0.0048		
0.550–0.600	0.4100±0.0031±0.0025		
0.600–0.650	0.2574±0.0025±0.0033	0.1516±0.0018± 0.0067	0.00041±0.00020± 0.00094
0.650–0.700	0.1720±0.0020±0.0027		
0.700–0.750	0.1042±0.0015±0.0026		
0.750–0.800	0.0608±0.0011±0.0027		
0.800–0.900	0.0263±0.0005±0.0032	0.0175±0.0005± 0.0057	−0.0002 ±0.0002 ± 0.0011
0.900–1.000	0.0049±0.0002±0.0020		

Table 1: Total, transverse and longitudinal inclusive cross section for charged particles, measured at $\sqrt{s} = 91.2$ GeV. The errors are the bin-to-bin errors, the first one being the statistical and the second one the systematic uncertainty. A normalization error of 1% has to be added in quadrature everywhere.

4 Results

The fragmentation functions for the different flavours and the gluon are parametrized using the functional form

$$x D_i(x, s_0) = N_i \, \frac{(1-x)^{a_i} x^{b_i} \exp\left(-c \ln^2 x\right)}{\int_{0.1}^{0.8} dx \, (1-x)^{a_i} x^{b_i} \exp\left(-c \ln^2 x\right)} \; ,$$

at a reference energy, $\sqrt{s_0}$. Here the index i represents, separately, light quarks, charm, bottom and gluons. The exponential function is motivated by the Modified Leading-Log Approximation (MLLA) [26, 27], which also predicts a single value of the c parameter for all quark flavours as well as the gluon. In total, thirteen parameters are used to describe the fragmentation functions at one energy. The evolution to another energy requires two more parameters: α_s, which determines the perturbative evolution, and h_0, which parametrizes the non-perturbative effects in the evolution. Finally, the effective leading-order coupling constant β_s introduced in eq. (3) is required. Altogether there are sixteen parameters, which are all fitted simultaneously to the available data.

An overall fit of the QCD predictions to all ALEPH data and the low energy data discussed above is performed. In the global fit the evolution of the all-flavour inclusive distributions available at the various centre-of-mass energies carries the information about the strong coupling α_s and the non-perturbative effects as parametrized by h_0. The flavour-tagged distributions measured by ALEPH at $\sqrt{s} = 91.2$ GeV mainly serve the purpose of fixing the parameters of the corresponding fragmentation functions. The gluon-tagged sample from ref. [15] and the longitudinal and transverse distributions determine β_s and the parameters of the gluon fragmentation function.

For the nominal analysis the value of $\sqrt{s_0}$ is chosen to be 22 GeV. The fit range was taken to be $0.1 < x < 0.8$ for all data at all energies. Outside this range, systematic effects, especially at low $\sqrt{s}$, start to become important. However, the fit range for the longitudinal cross section (measured only at 91.2 GeV), is taken to be $0.04 < x < 0.8$ to increase the statistical sensitivity.

The results of the fit are shown in Table 2. There are sizable correlations amongst most of the parameters, which may be as large as 90% between the parameters of the fragmentation functions. The parameter most strongly correlated with $\alpha_s(M_Z)$ is the one describing the energy evolution of the non-perturbative terms, h_0. Here the correlation is 36%. The value found for h_0 is compatible with zero, which indicates that non-perturbative effects are small, within the parametrization given by eq. (4). Fixing the parameters describing the shape of the fragmentation functions and the non-perturbative corrections, the purely experimental error of $\alpha_s(M_Z)$ would be $\Delta\alpha_s = 0.002$.

Figure 2 shows that the overall agreement between data and prediction is good and that the QCD evolution reproduces the observed scaling violations. The size of the scaling violations can be seen in Fig. 3, where the ratio between the inclusive cross sections measured at the extremes of the covered energy range is plotted as function of x. For comparison also the expectation with the flavour composition kept constant at the value at 91.2 GeV is given. The fitted gluon fragmentation function is displayed in Fig. 4 together with the direct measurement [15]. All error bars include both statistical and experimental systematic uncertainties. The value found for α_s agrees with previous ALEPH determinations [7, 28] and c with the MLLA expectation [27]. Also β_s is consistent with typical values for a leading-order α_s measurement. Since β_s is allowed to

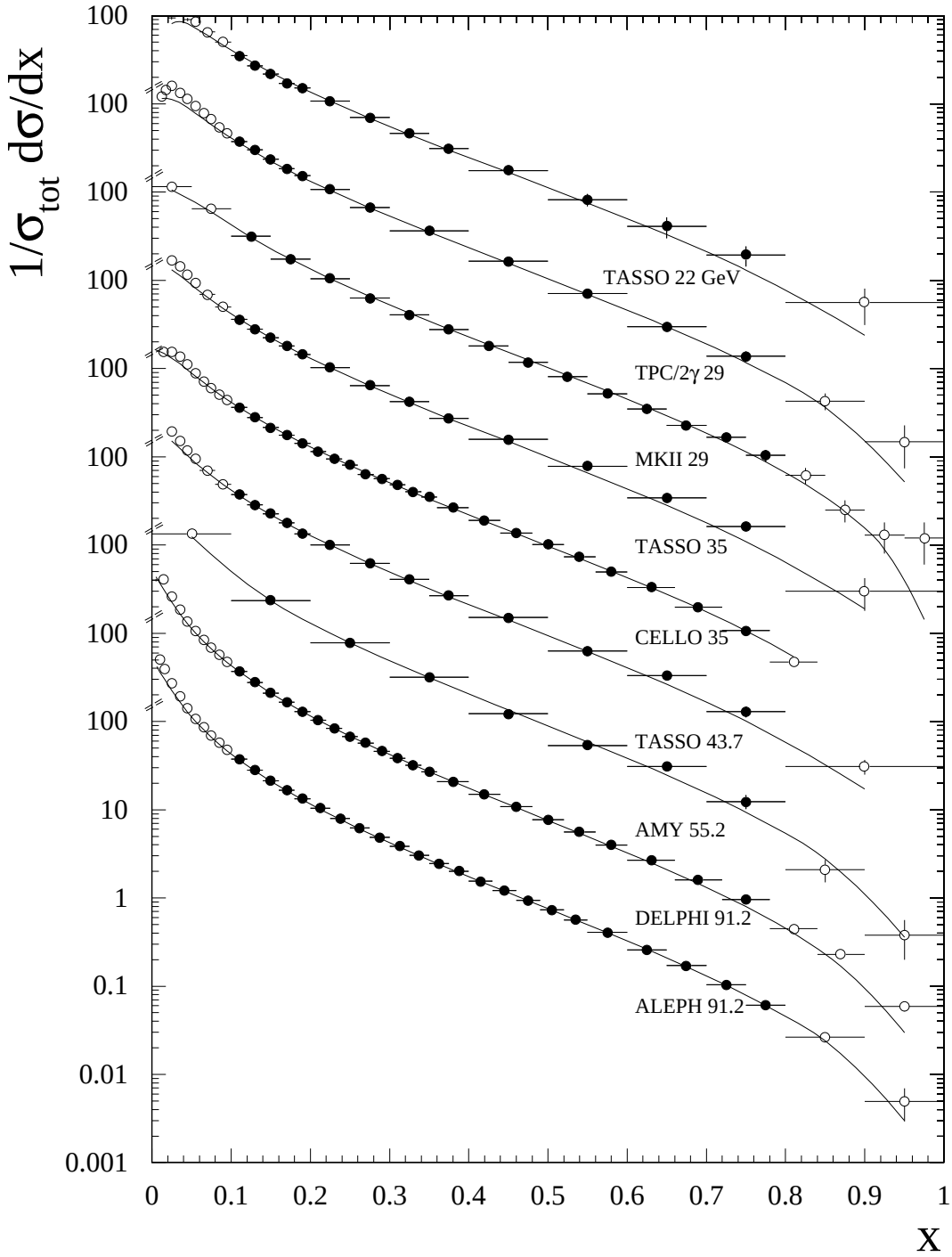

Figure 2: Inclusive all-flavour scaled-energy distributions used in the QCD fit. Only the full dots enter the fit. Errors shown include statistical and systematic uncertainties. The curves represent the results of the fit.

$\alpha_s(M_Z) = 0.1258 \pm 0.0053$ $h_0 = -0.14 \pm 0.10$ GeV				
	light (uds) quarks	c quarks	b quarks	gluons
N	0.372 ± 0.005	0.359 ± 0.006	0.295 ± 0.008	0.395 ± 0.020
a	1.69 ± 0.04	3.09 ± 0.16	3.29 ± 0.09	2.6 ± 0.8
b	-1.40 ± 0.06	-1.10 ± 0.09	-1.69 ± 0.07	-1.59 ± 0.29
c	0.252 ± 0.014			
β_s	0.199 ± 0.008			

Table 2: Results of the fit to all data. The errors include statistical and experimental systematic uncertainties, except for those related to flavour tagging. The parameters N_i, a_i, b_i and c define the shape of the fragmentation functions at the scale $\sqrt{s_0} = 22$ GeV. The definition of the parameters is given in the text.

vary, the information about the gluon fragmentation function obtained from the longitudinal cross section improves only marginally the direct measurement [15].

The χ^2 per degree of freedom (dof) of the fit is 307/213. Three distributions contribute substantially to the χ^2: MARK II (37/14), TASSO at 35 GeV (45/13) and the ALEPH b-enriched sample (65/23). The large χ^2 for the b quark enriched sample is due to inadequacies of the simple parametrization of the fragmentation function. While the simple ansatz is good enough to describe the fragmentation of the gluon and the light quarks including the c quark, it fails to reproduce the detailed structure of b quark fragmentation and decay over the full x range. Removing the high-x points above $x = 0.6$ changes the χ^2/dof to 29/19 while the result of the fit remains unchanged. The relatively high values of the χ^2 for MARKII and TASSO(35 GeV) point to an inconsistency in the experimental data, since there are data from other experiments at the same energy which are perfectly consistent with the QCD fits. In order to understand the importance of these problems for the fit, the errors of these two distributions are scaled up by the corresponding values of $\sqrt{\chi^2/\mathrm{dof}}$, effectively deweighting the results from those experiments. The results of the fit with the enlarged errors and the ALEPH b-enriched sample restricted to the range $0.1 < x < 0.6$ is $\alpha_s(M_Z) = 0.127 \pm 0.006$, fully consistent with the previous one, with an overall $\chi^2/\mathrm{dof} = 219/209$.

Most of the experimental part of the systematic errors in the α_s determination is already contained in the error obtained from the fit. The only remaining uncertainties are from the treatment of the normalization errors and the knowledge of the purities of the flavour-enriched samples.

The normalization errors pose a problem for those experiments where only the combined statistical and systematic errors have been published. In those cases the purely statistical error was estimated from the amount of data that was available and subtracted from the total errors. Of the remaining relative errors in the respective x bins, the minimum one was taken to be the normalization uncertainty common to all bins. This procedure was adopted for the nominal

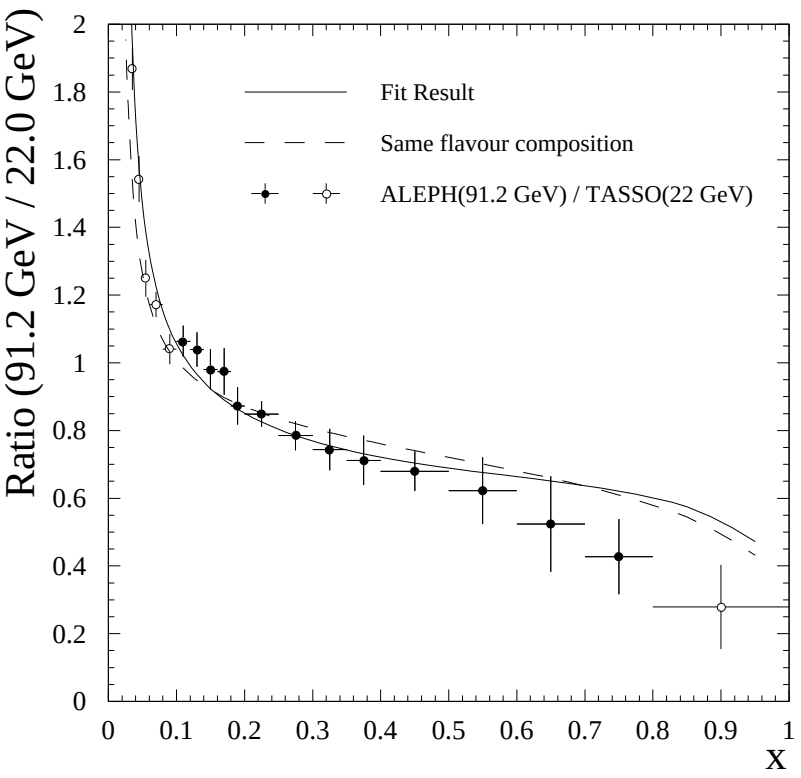

Figure 3: Ratio of inclusive cross sections at $\sqrt{s} = 91.2$ GeV and $\sqrt{s} = 22$ GeV compared to the QCD prediction. The full dots contributed in the global fit. The curves show the result of the fit to all distributions.

analysis. Alternatively all unspecified errors were taken as bin-to-bin errors and the resulting shift $\Delta\alpha_s = 0.002(norm)$ taken as an additional systematic error.

By varying the confidence-level cuts in the lifetime tags, the flavour compositions were changed such that the flavour enrichment for u, d, s and b quarks changed by $\pm 4\%$ and for c quarks by -4% and $+2\%$ (it was found to be very difficult to get higher purities). The maximum change was $\Delta\alpha_s = 0.004$, being equivalent to an uncertainty of $\pm 4\%$ in the purity estimates from the Monte Carlo. This shift was taken as the systematic error due to flavour composition of the tagged data samples. The total experimental error of $\alpha_s(M_Z)$ is $\Delta\alpha_s(exp) = \pm 0.005(fit) \pm 0.002(norm) \pm 0.004(purity)$.

Theoretical errors were determined, following [7], by varying independently the factorization and the renormalization scale in the range $-1 \leq \ln(\mu^2/s) \leq 1$. The resulting changes in $\alpha_s(M_Z)$ are $\Delta\alpha_s(theory) = \pm 0.002(\mu_R) \pm 0.006(\mu_F)$. Combining all errors in quadrature the final result for $\alpha_s(M_Z)$ becomes

$$\alpha_s(M_Z) = 0.126 \pm 0.007(exp) \pm 0.006(theory) = 0.126 \pm 0.009 \quad .$$

Several additional consistency checks were carried out. The parametrization scale was varied from $\sqrt{s_0} = 22$ GeV to 45 GeV or 91 GeV. The resulting changes on $\alpha_s(M_Z)$ were below 0.002 in all cases. Then the sensitivity to the assumption about the behaviour of the non-perturbative contributions was tested. Using the parametrization of eq.(4) with $1/s$ instead of $1/\sqrt{s}$ gave

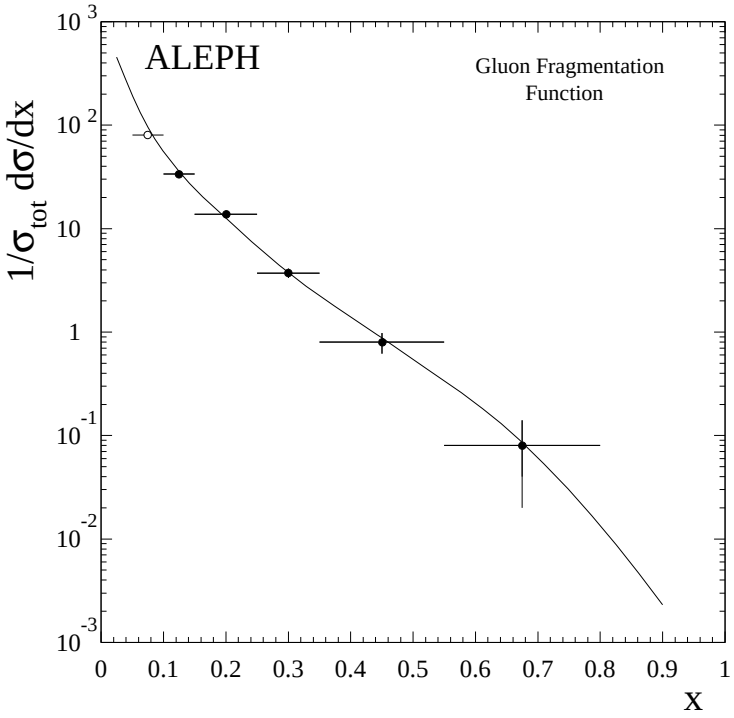

Figure 4: Direct measurement of the gluon fragmentation function for gluons with an average energy of $< E_g >= 24$ GeV [15] compared with the gluon fragmentation function obtained from the global fit, evaluated at a scale of 48 GeV. The full dots were used in the global fit.

completely negligible shifts in $\alpha_s(M_Z)$. Trying a rescaling ansatz as used in ref. [6]

$$x = x' \left[1 + h_1 \cdot \left(\frac{1}{\sqrt{s}} - \frac{1}{\sqrt{s_0}} \right) \right]$$

instead of eq. (4) to parametrize non-perturbative effects resulted in a correlation around 90% between α_s and h_1, thereby precluding a simultaneous measurement of both parameters. Fixing h_1 to the value estimated in ref. [6] from the HERWIG Monte Carlo, the result of the fit was compatible with the nominal result within the quoted uncertainties.

The dependence on the choice of the fit interval was studied by varying the lower bound of the fit range by ± 0.05 around the nominal value of $x_{min} = 0.1$. In both cases a value for $\alpha_s(M_Z)$ statistically compatible with the nominal result is obtained. The χ^2 of the fit degrades considerably when going to smaller x_{min}, indicating that the parametrization of the fragmentation functions and non-perturbative terms is not suitable for very small x. Going to much larger values of x_{min} amounts to giving up much of the available data, and the fit of all 16 parameters becomes unstable, with correlations of more than 90% between many of the variables.

Finally, the whole parametrization except $\alpha_s(M_Z)$ was fixed to the nominal result, and the strong coupling constant was fitted, using the same formalism as before, in independent x intervals of size $\Delta x = 0.1$ between $x = 0.1$ and $x = 0.8$. All results were found to be statistically compatible with the nominal one, verifying that scaling violations over the full x range are described by one single coupling constant.

5 Conclusions

The inclusive distribution $(1/\sigma_{tot})(d\sigma/dx)$ for charged particles has been measured by the ALEPH experiment for hadronic events of all flavours and enriched samples in light flavours, c quarks and b quarks. In addition, the transverse and longitudinal distributions were measured and, together with information from identified gluon jets, used to constrain the gluon fragmentation function.

A global analysis of these measurements and results from other experiments at lower centre-of-mass energies has been carried out in the framework of next-to-leading order QCD. Scaling violations in the time-like domain between $\sqrt{s}$ = 22 GeV and $\sqrt{s}$ = 91.2 GeV are observed in agreement with QCD predictions. The data are found to be consistent with one universal coupling constant describing the evolution of the fragmentation functions between $\sqrt{s} = 22$ GeV and $\sqrt{s} = 91.2$ GeV. At the same time, the shape of the fragmentation function for gluons, light flavours, c and b quarks were determined from the data alone.

The strong coupling constant measured here from scaling violations is consistent with other determinations [7, 28] at one fixed energy based on global event shape variables. Expressed at the scale M_Z, the measured value is $\alpha_s(M_Z) = 0.126 \pm 0.009$.

The main single contribution to the error on α_s comes from the dependence on the factorization scale chosen. Next-to-next-to-leading order calculations of the coefficient functions and splitting kernels would decrease this source of error. The overall error is bigger than for some other determinations of the strong coupling constant [4, 7] mainly because all non-perturbative effects (in the value of the fragmentation functions at one energy and in their evolution) have been taken directly from data, without relying on the quantitative predictions of the Monte Carlo models.

Acknowledgements

We would like to thank P. Nason and B. Webber for very helpful discussions and P. Aurenche for a very useful comment. It is a pleasure to thank our colleagues from the accelerator divisions for the continuously improved performance of the LEP machine. Thanks are also due to the engineers and technicians both at CERN and at our home institutions for their contribution towards the success of the experiment. Those of us from non-member states thank CERN for its hospitality.

References

[1] V. N. Gribov and L. N. Lipatov, Sov. J. Nucl. Phys. 15 (1972) 78;
G. Altarelli, G. Parisi, Nucl. Phys. B126 (1977) 298;
Yu. L. Dokshitzer, Sov. Phys. JETP 46 (1977) 641.

[2] G. Gurci, W. Furmanski and R. Petronzio, Nucl. Phys. B175 (1980) 27;
W. Furmanski and R. Petronzio, Phys. Lett. B97 (1980) 437.

[3] G. Altarelli, R. K. Ellis, G. Martinelli and So-Young Pi, Nucl. Phys. B160 (1979) 301.

[4] P. Abreu *et al.*, DELPHI Collab., Phys. Lett. B311 (1993) 408.

[5] T. Sjöstrand and M. Bengtsson, Comp. Phys. Comm. 43 (1987) 367;
M. Bengtsson and T. Sjöstrand, Phys. Lett. B185 (1987) 435.

[6] P. Nason and B. R. Webber, Nucl. Phys. B421 (1994) 473.

[7] D. Decamp *et al.*, ALEPH Collab., Phys. Lett. B284 (1992) 163.

[8] D. Decamp *et al.*, ALEPH Collab., Nucl. Instrum. Methods A294 (1990) 121.

[9] D. Buskulic *et al.*, ALEPH Collab., Nucl. Instrum. Methods A360 (1995) 481.

[10] D. Buskulic *et al.*, ALEPH Collab., Z. Phys. C55 (1992) 209.

[11] S. Jadach, J. H. Kühn and Z. Wąs, Comp. Phys. Comm. 64 (1991) 275;
S. Jadach, B. F. L. Ward and Z. Wąs, Comp. Phys. Comm. 66 (1991) 276.

[12] J. E. Campagne and R. Zitoun, Z. Phys. C43 (1989) 469.

[13] D. Buskulic *et al.*, ALEPH Collab., Phys. Lett. B313 (1993) 535.

[14] D. Buskulic *et al.*, ALEPH Collab., Phys. Lett. B313 (1993) 549.

[15] D. Buskulic *et al.*, ALEPH Collab., "Quark and Gluon Jet Properties in Symmetric Three-Jet Events", article in preparation; D. Buskulic *et al.*, ALEPH Collab., contribution to the 27th Intl. Conf. on High Energy Physics, Glasgow, Scotland, July 1994 (Ref. GLS0539).

[16] D. Decamp *et al.*, ALEPH Collab., Phys. Lett. B273 (1991) 181.

[17] K. Kato and T. Munehisa, Comp. Phys. Comm. 64 (1991) 67; Mod. Phys. Lett. A1 (1986) 345; Phys. Rev. D36 (1987) 61; Phys. Rev. D39 (1989) 156.

[18] G. Gustafson and U. Petterson, Nucl. Phys. B306 (1988) 746;
L. Lönnblad, preprint LU-TP 89-10.

[19] G. Marchesini and B. R. Webber, Nucl. Phys. B310 (1988) 461;
I. Knowles, Nucl. Phys. B310 (1988) 571;
G. Marchesini *et al.*, Comp. Phys. Comm. 67 (1992) 465.

[20] R. Akers *et al.*, OPAL Collab., CERN-PPE/95-057.

[21] W. Braunschweig *et al.*, TASSO Collab., Z. Phys. C47 (1990) 187.

[22] A. Petersen *et al.*, MARK II Collab., Phys. Rev. D37 (1988) 1.

[23] H. Aihara *et al.*, TPC/2γ Collab., Phys. Rev. Lett. 61 (1988) 1263; updated in G. D. Cowan, internal note TPC-LBL-94-01.

[24] O. Podobrin, CELLO Collab., Ph.D. thesis, Universität Hamburg. See also ref. [4].

[25] Y. K. Li *et al.*, AMY Collab., Phys. Rev. D41 (1990) 2675.

[26] See, for instance, Yu. L. Dokshitzer, V. A. Khoze, A. H. Mueller and S. I. Troyan, *Basics of Perturbative QCD*, Editions Frontières, Gif-sur-Yvette (France), 1991; and references therein.

[27] C. P. Fong and B. R. Webber, Nucl. Phys. B355 (1991) 54.

[28] D. Decamp *et al.*, ALEPH Collab., Phys. Lett. B255 (1991) 623; Phys. Lett. B257 (1991) 479.